ARTICLE

Check for updates

Directional ionic transport across the oxide interface enables low-temperature epitaxy of rutile TiO$_2$

Yunkyu Park[1], Hyeji Sim [1], Minguk Jo[1], Gi-Yeop Kim[1], Daseob Yoon[1], Hyeon Han [1,2], Younghak Kim[3], Kyung Song[4], Donghwa Lee [1], Si-Young Choi [1] & Junwoo Son [1✉]

Heterogeneous interfaces exhibit the unique phenomena by the redistribution of charged species to equilibrate the chemical potentials. Despite recent studies on the electronic charge accumulation across chemically inert interfaces, the systematic research to investigate massive reconfiguration of charged ions has been limited in heterostructures with chemically reacting interfaces so far. Here, we demonstrate that a chemical potential mismatch controls oxygen ionic transport across TiO$_2$/VO$_2$ interfaces, and that this directional transport unprecedentedly stabilizes high-quality rutile TiO$_2$ epitaxial films at the lowest temperature ($\leq 150\,°C$) ever reported, at which rutile phase is difficult to be crystallized. Comprehensive characterizations reveal that this unconventional low-temperature epitaxy of rutile TiO$_2$ phase is achieved by lowering the activation barrier by increasing the "effective" oxygen pressure through a facile ionic pathway from VO$_{2-\delta}$ sacrificial templates. This discovery shows a robust control of defect-induced properties at oxide interfaces by the mismatch of thermodynamic driving force, and also suggests a strategy to overcome a kinetic barrier to phase stabilization at exceptionally low temperature.

[1] Department of Materials Science and Engineering (MSE), Pohang University of Science and Technology (POSTECH), Pohang 37673, Republic of Korea.
[2] Max Planck Institute of Microstructure Physics, Weinberg 2, Halle (Saale) 06120, Germany. [3] Pohang Accelerator Laboratory, Pohang 37673, Republic of Korea. [4] Materials Modeling and Characterization Department, Korea Institute of Materials Science (KIMS), Changwon, Republic of Korea.
✉email: jwson@postech.ac.kr

nterfaces formed by two dissimilar materials can break the translational symmetry and thereby provide an opportunity to develop functionality that is unachievable in bulk materials[1–5]. When two materials (I, II) that have different work functions (i.e., $\mu_e^I < \mu_e^{II}$) are brought together at a semiconductor heterojunction, charge carriers near the interface diffuse across the junction (Fig. 1a);[1,2] as a consequence, a conducting channel with high carrier density and high electron mobilities (e.g., two-dimensional electron gas) could be created at the interfaces between normally-insulating materials[2,3]. If an external bias is applied to adjust this built-in potential, the amount of transferred charge flow can be controlled by changing the electrochemical potential across chemically-inert interfaces[2,6], which is the basic principle of heterojunction field effect transistors (HFETs)[7].

As an analogy to the reversible control of electric charge transfer at an interface with discontinuity, (electro-)chemical potential mismatch for oxygen ($\Delta\mu_O$) between two materials ($\mu_O^I < \mu_O^{II}$) may give rise to charged ionic transfer to bring the equilibrium of the system with heterogeneous junction at the interface (Fig. 1a)[5,8–12]. In particular, charged ionic defects migrate by ionic diffusion (e.g., diffusion of oxygen ions through vacancies) to mitigate $\Delta\mu_O$ at the interface;[9–14] charged ions, in principle, are transferred to adjacent materials and reconfigured by the redox reaction across the chemically-reacting interfaces in oxide heterostructure until the chemical potentials of the layers match ($\mu_O^I = \mu_O^{II}$ in Fig. 1a)[5].

For example, the vanadium dioxide (VO_2), the archetypal correlated oxide with metal-insulator (MI) transition near room temperature, is interfaced with ionic liquid (IL), and then (electro-)chemical potential can be adjusted by applying an external electric field across the VO_2/IL interfaces[9,14–16]. In this case, instead of electric charge transfer, charged oxygen ions out-diffused to the IL to equilibrate the (electro-)chemical potential between VO_2 and IL; the formation of oxygen vacancies (V_O) by oxygen ion migration are responsible for the reversible insulator-to-metal transition and giant lattice expansion in VO_2 films under the positive bias[15]. Furthermore, V_O concentrations that develop in $LaNiO_3$, $LaTiO_3$, and In_2O_3 can be modulated by the directional oxygen flow to the adjacent layers[10–12].

At interfaces where ionic flux ($J_{O^{2-}}$ in Fig. 1a) is directional, the dynamics of charged ions may be important by assembling other metal oxides that have different μ_O[10,11,14]. The redistribution of charged vacancies can screen the electric fields that $\Delta\mu_O$ causes. Therefore, the massive redistribution of charged ions can be accelerated by extremely increasing the thermodynamic $\Delta\mu_O$ across the interfaces; by supplying unidirectional charged ionic flux, this redistribution may offer a spontaneous route that can facilitate synthesis of crystalline materials[12], and may enable robust control of defect-induced properties at oxide interfaces[9,13,14].

Here, we demonstrate the formation of high-quality rutile TiO_2 epitaxial films at exceptionally low temperature, which is driven by directional transport of oxygen ions across the TiO_2/VO_2 heterointerfaces. Contrary to the amorphous nature of TiO_2 films directly grown on TiO_2 substrates at 150 °C, single-crystal rutile TiO_2 layer is synthesized by forming the heterointerface with VO_2 template at the lowest growth temperature T_G (<150 °C) ever reported, at which rutile TiO_2 is difficult to be crystallized. By
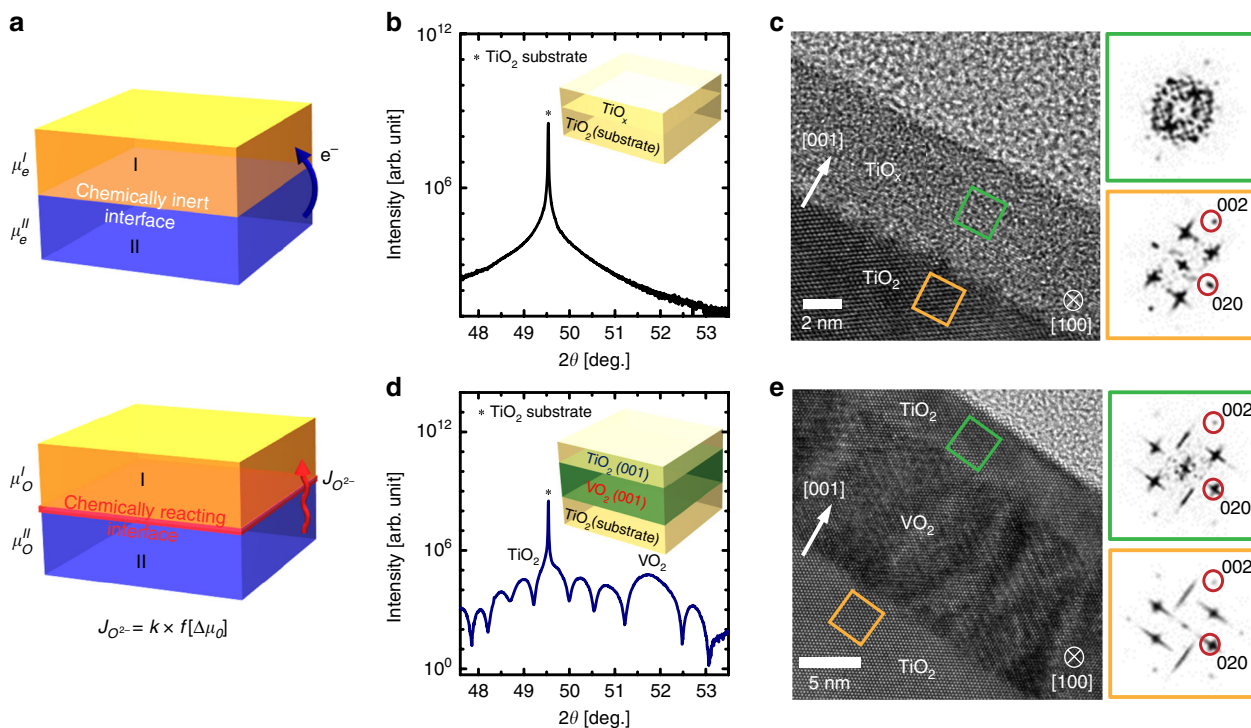

Fig. 1 Low-temperature epitaxy of rutile TiO_2 on VO_2 sacrificial templates. a Schematics of possible directional charge (top) and ionic (bottom) transport due to chemical potential mismatch ($\Delta\mu$) across the interface with loss of translational symmetry. Symmetrical x-ray scan of **b** TiO_X/TiO_2 homostructure and **d** TiO_2/VO_2/TiO_2 heterostructure containing TiO_2 films grown at 150 °C. Contrary to the absence of peak around TiO_2 substrate peak in homostructure (**b**), (002) Bragg reflections and Kiessig fringes around the peak from TiO_2 substrate in heterostructure in **d** indicate that the TiO_2 films are epitaxially grown at 150 °C on VO_2 templates with sharp interface. HRTEM images and FFT patterns of **c** TiO_X/TiO_2 homostructure (scale bar = 2 nm) and **e**. TiO_2/VO_2/TiO_2 heterostructure (scale bar = 5 nm) projected with [100] zone axis. Unlike the amorphous nature of TiO_X films in homostructures (green square in **c**), obvious diffraction spots were observed in the FFT pattern of the TiO_2 films on VO_2/TiO_2 (green square in **e**), and were same as those observed from the TiO_2 substrates (yellow square in **e**); this similarity indicates an identical epitaxial relationship of TiO_2 epitaxial films with TiO_2 substrates in TiO_2/VO_2/TiO_2 heterostructure.

experimental characterization using atomic-resolution electron microscopy and synchrotron x-ray spectroscopy combined with theoretical calculation, we demonstrate that a facile ionic diffusion of oxygen ions from the oxygen reservoir VO_2 along the [001] channel decreases $\Delta\mu_O$, and thereby enables this unprecedented epitaxy of rutile TiO_2 at low temperature by lowering the activation barrier for formation of stable nuclei. Interestingly, this directional ionic transport improves the registry in the lattice of TiO_2 films at the expense of the structural and electronic modulation in an oxygen-deficient $VO_{2-\delta}$ sacrificial layer. As a result of the mismatch of thermodynamic driving force combined with kinetically-facile migration of oxygen ions across the TiO_2/VO_2 interfaces, the massive redistribution of oxygen ions enables low-temperature epitaxy of high-temperature-stabilized phase by increasing an "internal" oxygen supply across the chemically-reacting oxide interface.

Results

Low temperature epitaxial growth of rutile TiO_2 films on VO_2 template. Prior to TiO_2 growth, the substrates with 12-nm-thick VO_2 template were prepared on (001)-oriented TiO_2 substrates by pulsed laser deposition (Supplementary Fig. 1). X-ray diffraction (XRD) results (Supplementary Fig. 2a) showed sharp VO_2 $(002)_R$ peaks (in rutile notation) at $\sim 2\theta = 65.9°$ ($c = 0.2839$ nm) without other peaks related to vanadium oxides that had valence states other than +4. A steep MI transition ($\Delta R_S \sim 10^{3.3}$) occurred on the VO_2 films at $T_{MI} \sim 298$ K (Supplementary Fig. 2b); this result indicates the formation of coherently tensile-strained VO_2 films with high crystal quality and negligible V_O[9,15,17,18].

Then, the 6 nm-thick TiO_2 films were grown at low $T_G \sim 150\,°C$ with the same oxygen pressure ($pO_2 \sim 12$ mTorr) on two substrates: 1) (001) TiO_2 single crystals without the VO_2 template layer (denoted as TiO_2/TiO_2 hereafter) and 2) (001) TiO_2 single crystals with the VO_2 template (denoted as $TiO_2/VO_2/TiO_2$). Symmetric 2θ-ω scans using synchrotron X-ray scattering on TiO_2/TiO_2 grown at $T_G = 150\,°C$ (Fig. 1b) detected no Bragg reflections except for substrate ($2\theta = 49.54°$); this absence indicates no formation of crystalline TiO_2 films[16]; the formation of amorphous TiO_2 films on TiO_2 substrates is attributed to the thermodynamic or kinetic instability of the rutile TiO_2 phase, which requires sufficient thermal energy for phase formation[19–23]. To exclude the possible coincidence of diffraction peak from TiO_2 films and substrates in homostructures in Fig. 1b, TiO_2 films were also grown on (100) Al_2O_3 single crystal substrates (Supplementary Fig. 3). The symmetric 2θ-ω scan in wide range of angle also detected the only peak related to the (100) Al_2O_3 substrate ($2\theta = 68.22°$) due to the formation of amorphous films at $T_G = 150\,°C$.

In contrast, rutile TiO_2 epitaxial films were strikingly stabilized by introducing the VO_2 layers on TiO_2 substrate at the same condition with $T_G = 150\,°C$. Symmetric 2θ-ω scans of $TiO_2/VO_2/TiO_2$ heterostructures (Fig. 1d) showed two Bragg reflections, one from the rutile TiO_2 ($2\theta = 49.46°$) substrates, and one from VO_2 ($2\theta = 51.8°$) films. More importantly, the TiO_2 substrate peak was resolved to a slightly broad peak from TiO_2 epitaxial films[16], which did not appear in the scans of TiO_2/TiO_2 homostructure. Each film peak exhibited a Kiessig fringe; fitting of the peaks showed that their periodicity differed due to different film thickness (Supplementary Fig. 4); these clear oscillations from peaks represent sharp interface of $TiO_2/VO_2/TiO_2$ all-epitaxial heterostructures.

The low-temperature epitaxy of rutile TiO_2 films on VO_2-templated substrates was locally visualized by comparing cross-section high-resolution transmission electron microscope (HRTEM)

images of both TiO_x ($x < 2$)/TiO_2 and $TiO_2/VO_2/TiO_2$ (Fig. 1c, e). Amorphous nature of TiO_x films on TiO_2 was confirmed by the diffused halo feature in fast Fourier transform (FFT) pattern from the films (green square in the right column of Fig. 1c). In contrast, sharp diffraction spots were observed in FFT pattern of the TiO_2 films on VO_2/TiO_2 (green square in the right column of Fig. 1e), and is similar with that from the TiO_2 substrates (yellow square in the right column of Fig. 1e); this observation demonstrates that epitaxial rutile TiO_2 films can be crystallized at 150 °C simply by introducing VO_2 templates on TiO_2 substrate. Considering the dramatic difference of crystallinity in those TiO_2 films grown at the same growth condition, the epitaxial TiO_2 with excellent crystallinity at 150 °C is unusual, because it formed even though thermal energy was insufficient at 150 °C to overcome the activation energy that is required to drive formation of thermodynamically stable crystalline nuclei[20,23].

To determine how this unprecedented rutile TiO_2 phase developed low-temperature epitaxy, annular bright field (ABF) scanning transmission electron microscopy (STEM) data were analyzed with $TiO_2/VO_2/TiO_2$ heterostructure. The sensitivity of ABF to light-weight atoms permitted visualization of oxygen atomic columns in ABF STEM (Fig. 2a)[17]. Magnified ABF-STEM images (red rectangles) show the typical rutile TiO_2 structure in both film and substrate; this result indicates that TiO_2 films had been fully crystallized by coherent epitaxial growth on VO_2 templates. However, the contrasts of oxygen atomic columns in VO_2 are weak and diffuse in the enlarged images of VO_2 (blue rectangle); this result implies that oxygen contents are deficient in the VO_2 template after low-temperature epitaxy of stoichiometric rutile TiO_2 films. Therefore, TiO_2 films with perfect registry of atoms were epitaxially grown on top of defective VO_2 templates; this result is contrary to the general principle that high-quality epitaxial growth is achieved by using low-defect substrates, and suggests that the chemical reaction at the interface is likely to facilitate the low-temperature epitaxy of high-quality TiO_2 films by sacrificing the initially good quality of VO_2 templates.

The formation of defective features in VO_2 template could be confirmed by comparing high-angle annular dark field (HAADF) and low-angle annular dark field (LAADF) signals of $TiO_2/VO_2/TiO_2$ heterostructures from STEM. Contrary to almost identical HAADF contrast across the heterostructures due to similar cation atomic weight across the heterostructures[16] (Fig. 2b), the LAADF contrast was noticeably mottled in VO_2 templates (Fig. 2c) that were sandwiched between TiO_2 films and substrates. The HAADF and LAADF images had distinct intensity profiles along the film growth direction of [001] (insets in Fig. 2b, c) The differences occur because the LAADF signal is more sensitive than the HAADF signal to the frustrated atomic channeling due to oxygen vacancies (V_O)[4,24], so the contrast is blurred and brighter in the LAADF signal of VO_2 templates. Moreover, electron energy loss spectroscopy (EELS) experiments reveal that the t_{2g} peak of O-K edge was strongly suppressed in the entire VO_2 template (Supplementary Fig. 5b); this result directly visualize the formation of oxygen vacancies[25]. Therefore, the combined results from LAADF contrast and EELS data in VO_2 templates confirms the significant loss of oxygen atoms from VO_2 during the low-temperature epitaxial growth of TiO_2 films in the heterostructures.

Suppression of metal-insulator transition in VO_2 templates by directional oxygen transport. Interestingly, the degree of oxygen deficiency of VO_2 templates was sensitively modulated by adjusting pO_2 (6 mTorr $\sim$ 24 mTorr) during TiO_2 growth at $T_G \sim$ 150 °C on VO_2-templated TiO_2 substrates. As observed in symmetric 2θ-ω synchrotron XRD scans in all heterostructures, Bragg
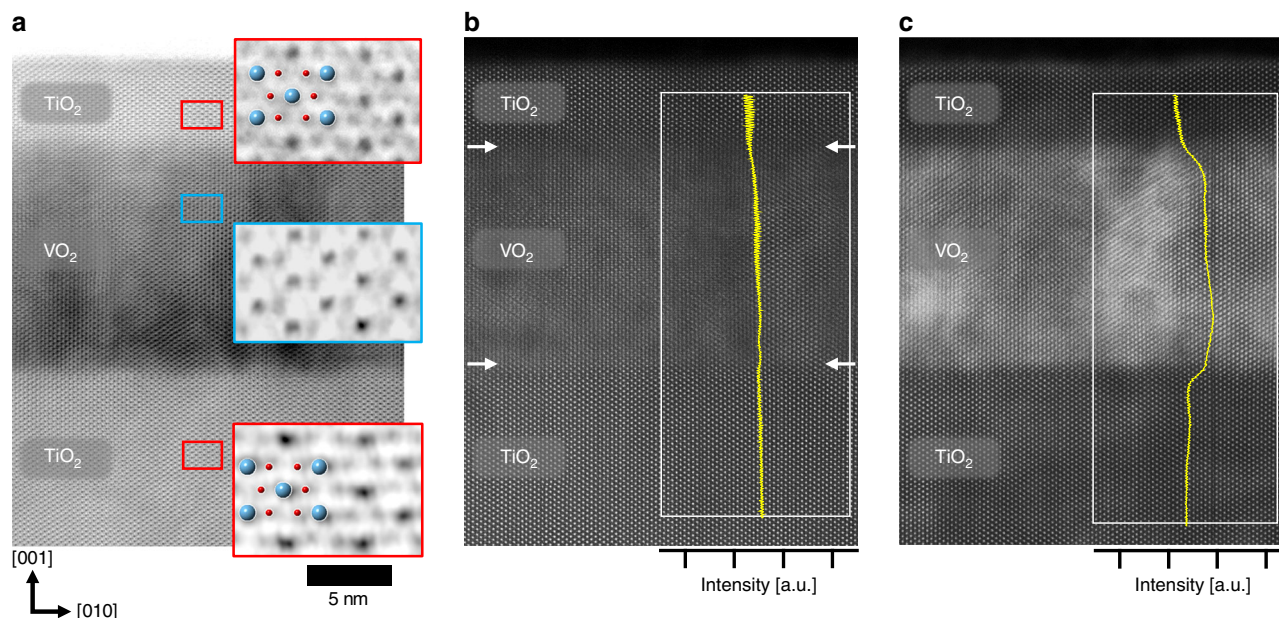
Fig. 2 Atomic-resolution analysis of TiO$_2$/VO$_2$/TiO$_2$ heterostructure. a ABF-STEM, **b** HAADF-STEM and **c** LAADF-STEM images of rutile TiO$_2$ epitaxial film grown on VO$_2$ sacrificial template at T_G = 150 °C with [100] zone axis (scale bar = 5 nm). The sensitivity of ABF technique to light-weight atoms enables observation of oxygen atoms along the [100] zone axis. Note that the regular pattern from TiO$_2$ epitaxial films (top red square in **a**) was identical to that from TiO$_2$ substrates (bottom red square in **a**), indicating an identical atomic arrangement of films with single crystals by epitaxial growth without oxygen defects. On the contrary, the oxygen-deficient region was observed in the sacrificed VO$_2$ template near the TiO$_2$ film (blue square in **a**). While almost-uniform HAADF contrast was observed across the heterostructures due to similar cation atomic weight across the heterostructures (**b**), a noticeable strain-field-induced LAADF contrast was observed in VO$_2$ templates (**c**) sandwiched between TiO$_2$ films and substrates. Yellow lines in **b** and **c** are the contrast-intensity profiles of the HAADF and LAADF images from the white rectangular areas.

peaks and Kiessig fringes from TiO$_2$ films were resolved from those from TiO$_2$ substrates and VO$_2$ templates with different period of oscillations in fringes (Fig. 3a), which again confirms the importance of VO$_2$ templates for low-temperature epitaxy of TiO$_2$ layers. However, unlike the almost identical peak of TiO$_2$ films and substrates, the (002) reflection of 14-nm-thick VO$_2$ template films decreased from $2\theta = 51.9°$ (black) to $2\theta = 51.5°$ (green) from symmetric 2θ-ω scans as pO_2 was reduced from 24 mTorr to 6 mTorr during the TiO$_2$ growth (Fig. 3a); this peak shift corresponds to ~ 0.8 % expansion of the out-of-plane lattice parameters in VO$_2$ templates.

For more detailed structural modulation of TiO$_2$/VO$_2$/TiO$_2$ heterostructures, reciprocal space mapping (RSM) around the (112) reflection of (001) TiO$_2$ substrate was performed to obtain the information on both in-plane and out-of-plane lattice parameters by adjusting pO_2 during TiO$_2$ growth (Fig. 3b). The RSM data of all heterostructures clearly show sharp and intense (112) Bragg reflections and Kiessig fringes from TiO$_2$ substrate and film, and from the VO$_2$ films. The substrate and film peaks showed identical H (i.e., in-plane reciprocal space unit)[26,27], which implicates that entire layers in all heterostructures are coherently strained by TiO$_2$ substrates along the in-plane direction. Geometric phase analysis (GPA) strain quantification using obtained STEM image confirms coherent interfaces through the heterostructures (Supplementary Fig. 6). However, only the VO$_2$ peak shifted to lower scattering angle (i.e., characteristic of expansion of out-of-plane lattice parameters) as the pO_2 during TiO$_2$ growth was decreased; these trends are consistent with vanadium valence state switching (V^{4+} to V^{3+}) by the formation of V_O in VO$_2$ templates[15,16,28].

Temperature-dependent sheet resistance R_S (T) of TiO$_2$/VO$_2$/TiO$_2$ heterostructures (by van der Paw methods) was measured to quantify how the accelerated oxygen deficiency in VO$_2$ templates

affected electrical transport of the heterostructures (Fig. 3c). The heterostructure that had been formed using pO_2~ 24 mTorr during TiO$_2$ growth (denoted as H24mT hereafter) exhibited slightly suppressed MI transition in terms of R_S(T) (i.e., ~ 3.2 orders of magnitude at T_{MI} ~ 298 K) compared with as-grown VO$_2$ films without TiO$_2$ layers on top. On the contrary, R_S(T) of the heterostructure with pO_2 of 6 mTorr (denoted as H6mT) substantially dropped by just less than an order of magnitude; This result indicates that MI transition of VO$_2$ templates was progressively suppressed and T_{MI} was monotonically decreased from 298 K (H24mT) to 260 K (H6mT) by the gradual increase of V_O in VO$_2$ as the TiO$_2$ films were grown at progressively lower pO_2 (Fig. 3d)[4,9]. As a result, the formation of V_O by oxygen ionic transfer across the interface not only expanded the lattice to compensate for the larger cation radius of V^{3+} (3d^2) than V^{4+} (3d^1)[28], but also induced the metallic state at TiO$_2$/VO$_2$ interfaces even at 270 K (Fig. 3e). Structural and electrical modulation driven by V_O in VO$_2$ cannot be generated by simple post-annealing without TiO$_2$ layer growth on top; directional oxygen ionic transport indeed occurs across the TiO$_2$/VO$_2$ interfaces by forming V_O in VO$_2$ layer, as long as TiO$_2$ layers are grown on VO$_2$ templates (Supplementary Fig. 14).

To elucidate the origin of metallicity in a VO$_2$ template interfaced with a TiO$_2$ layer, we performed polarization-dependent x-ray absorption spectroscopy (XAS) at the V $L_{2,3}$-edges for two heterostructures that contained 2.5-nm-thick TiO$_2$ films grown on VO$_2$ templates under pO_2 = 24 mTorr (H24mT, Fig. 4a) and 6 mTorr (H6mT, Fig. 4b). The XAS signals at the V $L_{2,3}$-edges represent a dipole-allowed transition from the V $2p_{1/2}$ and $2p_{3/2}$ core level to the V $3d$ valence electronic states (i.e., $2p^63d^1 \rightarrow 2p^53d^2$)[29–31] only from the VO$_2$ templates buried under layers of rutile TiO$_2$ owing to its element-specific character. Linearly-polarized X-rays with the polarization vector
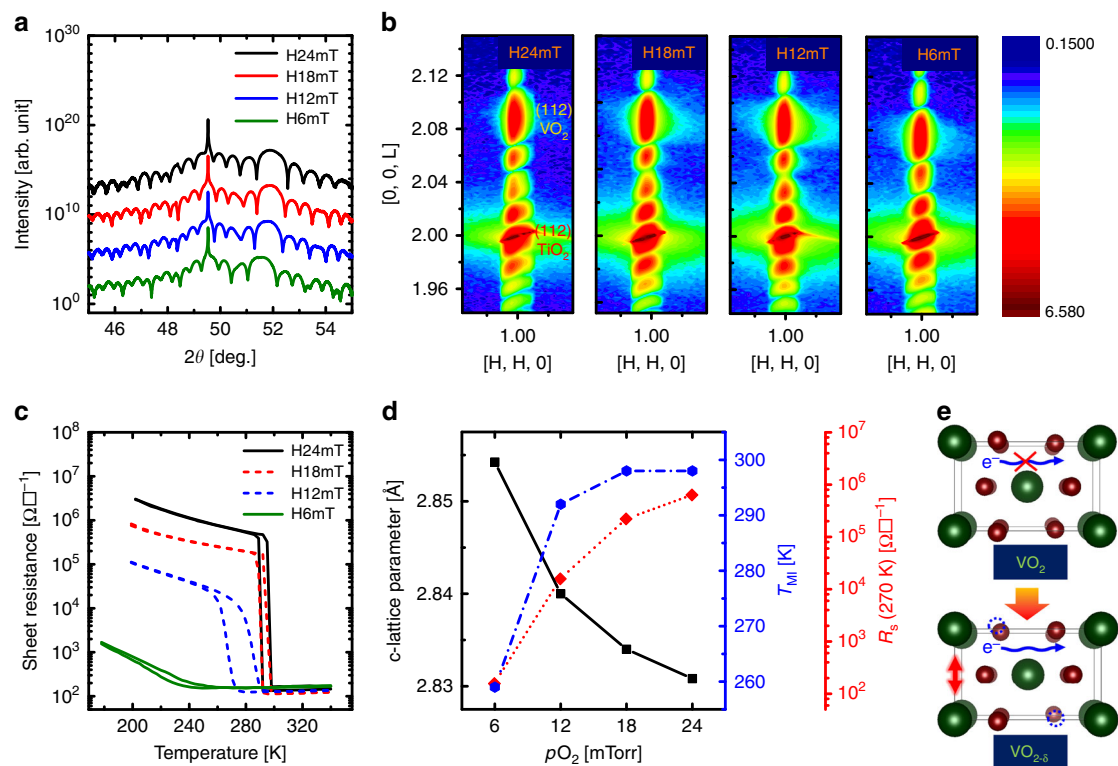
Fig. 3 Structural/electronic modulation by directional ionic transport. a Symmetrical X-ray scan and **b** reciprocal space mapping around (112) reflection of TiO$_2$ grown under pO_2 = 6 mTorr (denoted as H6mT) ~ 24 mTorr (denoted as H24mT) on VO$_2$-templated TiO$_2$ substrates. These results confirm that entire layers in all heterostructures are coherently strained by TiO$_2$ substrates, but only VO$_2$ peaks shifted to lower scattering angles as pO_2 decreased during TiO$_2$ growth. **c** Temperature-dependent sheet resistance (R_S) in all TiO$_2$/VO$_2$/TiO$_2$ heterostructures with TiO$_2$ epitaxial films grown at $6 \leq pO_2 \leq$ 24 mTorr on VO$_2$-templated TiO$_2$ substrates. **d** Lattice parameter (c) from **a** and temperature (T_{MI}) of metal-insulator transition and R_S at 270 K from **c** as a function of pO_2 during TiO$_2$ growth. **e** The formation of oxygen vacancies in VO$_2$ by ionic transfer across the TiO$_2$/VO$_2$ interface expanded the lattice to compensate for the larger cation radius of V^{3+} ($3d^2$) than V^{4+} ($3d^1$), and also led to the oxygen-vacancy-induced metallization.

parallel ($\mathbf{E}\|c$) and perpendicular ($\mathbf{E}\perp c$) to the out-of-plane orientation (c axis), respectively, detect the vacant $d_\|$ and π^* electron states[31], so V_O formation also significantly affects the dichroic signal (Fig. 4a, b) related to selective orbital occupancy of $d_\|$ induced by V-V dimerization[30,31].

In H24mT sample, XAS spectra collected at 320 K ($T > T_{MI}$) were similar regardless of the polarization direction of the X-ray (Supplementary Fig. 7a); this result was expected because of the isotropic orbital filling in the metallic states of VO$_2$ due to the absence of V-V dimerization. At 270 K ($T < T_{MI}$, Fig. 3c), X-ray linear dichroism (XLD, $I_\| - I_\perp$) was much larger than at $T = 320$ K (Fig. 4a, c); this increase is a signature of orbital polarization, which is expected to result from the strong V-V dimerization in the insulating states, due to the selective filling of $d_\|$ orbitals in VO$_2$ films with negligible oxygen loss (inset, Fig. 4c)[30,31]. In contrast, XAS spectra of H6mT, which is the sample with the highest driving force for oxygen ion transport from VO$_2$ sacrificial template, show no polarization-dependence of incident X-ray (Fig. 4d) at either $T = 270$ K (Fig. 4b) or 320 K (Supplementary Fig. 7b). This result indicates that selective filling of $d_\|$ orbitals did not occur below 270 K[30,31] and explains the V_O-induced metallic behavior at 270 K in H6mT: V_O tends to increase the crystal symmetry toward thermally-induced tetragonal rutile structure by weakening of V-V dimerization[15,32,33] and leads to isotropic orbital occupancy of $d_\|$ and π^*[33], (inset of Fig. 4d). The absence of selective filling in $d_\|$ orbitals in H6mT samples provides strong evidence for V_O formation in the entire area of sacrificial VO$_2$ templates by directional oxygen transport from VO$_2$ to TiO$_2$.

Stoichiometric TiO$_2$ epitaxy induced by directional oxygen transport. To explore the influence of directional ionic transport on the quality of TiO$_2$ epitaxial layer grown at T_G ~ 150 °C, we evaluated the element-specific Ti $L_{2,3}$-edge XAS signal from the TiO$_2$ layer in TiO$_2$/VO$_2$ heterostructures. The Ti L_3 edge peak between 457.9 eV ~ 461.3 eV (i.e., related to e_g orbitals) is split into two peaks due to the distortion of the TiO$_6$ octahedra in rutile structure; the relative intensities of these e_g doublet ($e_g^1 <$ e_g^2) verified a rutile TiO$_2$ phase in both H24mT and H6mT films[34,35] (Fig. 5a), which is consistent with our results in HRXRD and STEM. The Ti $L_{2,3}$-edge signals from H6mT were more intense and sharper than from H24mT[36,37]. Furthermore, the contribution of Ti^{3+} L-edge signals slightly increased the dips at 458 eV and 461 eV in the H24mT relative to those in H6mT (inset of Fig. 5a, yellow arrow)[36]; these results reveal that rutile TiO$_2$ films toward the stoichiometry with low oxygen deficiency can be formed more easily by the TiO$_2$ growth with low pO_2 than with high pO_2. Moreover, EELS data from the top TiO$_2$ layers in H6mT show that the t_{2g} peaks of Ti-L edge from TiO$_2$ layers is exactly same as those from stoichiometric bulk TiO$_2$ substrates (reference) (Supplementary Fig. 5c); this result represents the formation of stoichiometric TiO$_2$ layers at the expense of oxygen deficiency in VO$_2$ layers.

In addition to bulk-sensitive XAS and EELS, X-ray photoelectron spectroscopy (XPS) of the Ti $2p$ core level shows better stoichiometry of rutile TiO$_2$ film surface grown on VO$_2$ templates under low pO_2 than under high pO_2 (Fig. 5b). Deconvolution of The Ti $2p$ core-level peaks with Ti^{4+} ($2p_{3/2}$ ~ 458.8 eV, $2p_{1/2}$ ~ 464.6 eV) and Ti^{3+} ($2p_{3/2}$ ~ 457.2 eV, $2p_{1/2}$ ~ 463.1 eV) valence
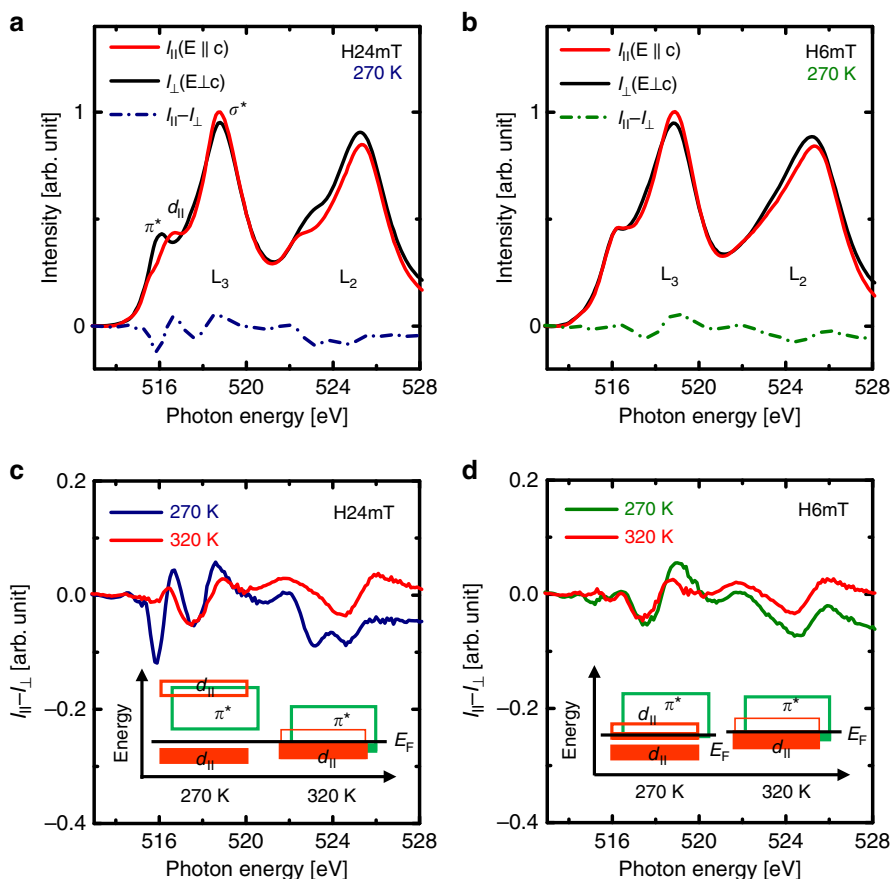
Fig. 4 Oxygen-vacancy-induced isotropic orbital occupancy in VO$_2$ templates. Polarization-dependent x-ray absorption spectroscopy (XAS) at the V $L_{2,3}$-edges at 270 K for two heterostructures composed of 2.5-nm-thick TiO$_2$ films grown on VO$_2$ templates under different pO_2 (**a** H24mT, **b** H6mT). Unlike large difference of XAS signal in H24mT at 270 K due to the orbital polarization with V-V dimerization in the monoclinic VO$_2$, almost no effect on the XAS signal in H6mT was observed at 270 K; this result indicates isotropic orbital filling in H6mT sample even at 270 K. The XLD ($I_\parallel$ – $I_\perp$) are also shown at both 270 K and 320 K for **c** H24mT and **d** H6mT. Oxygen vacancies driven by directional ionic transport in H6mT tend to increase the crystal symmetry to close to rutile structure by weakening of V-V dimerization, so selective filling of $d_\parallel$ (inset of **c**.) changes to isotropic orbital occupancy of $d_\parallel$ and π^* (inset of **d**) in VO$_2$ templates; the oxygen-vacancy-driven isotropic occupancy leads to metallization at 270 K.

states[38] showed negligible Ti^{3+} contribution from the H6mT was observed compared to H24mT in TiO$_2$/VO$_2$ heterostructures, which reveals the suppression of V_O formation even at the surface of TiO$_2$ resulting from enhanced oxygen transport across TiO$_2$/VO$_2$ interface under low pO_2; Both XAS and XPS results contradict the typical observation that stoichiometry could be improved in TiO$_2$ under high pO_2 by removing V_O[21,39].

Discussion

This study presents two interesting observations. (1) The increase in directional oxygen transport from VO$_2$ to TiO$_2$ with decrease in pO_2 during TiO$_2$ growth, and (2) facile formation of rutile TiO$_2$ epitaxial layer at extremely low temperature (≤150 °C). To identify the driving force for spontaneous oxygen loss from VO$_2$ templates, firstly, density functional theory (DFT) calculations were performed to determine values of the lower and upper limit of the chemical potential of oxygen (μ_O) for TiO$_2$ and VO$_2$ formation in general:

$$\frac{1}{2}\left(E_{tot}[TiO_2(or\ VO_2)] - \mu_{Ti}[Ti(or\ V)]\right) \leq \mu_O[TiO_2(VO_2)] \leq \mu_O[O_2]. \tag{1}$$

Our calculations predict that the lower limit of μ_O is −8.767 eV for VO$_2$ and −9.624 eV for TiO$_2$ (top of Fig. 5c), which indicates that TiO$_2$ is the only stable compound at −9.624 eV ≤ μ_O ≤ −8.767 eV. In the specific μ_O region in which VO$_2$ is thermodynamically

unstable, oxygen atoms can preferentially migrate from it to stable TiO$_2$.

Indeed, VO$_2$ and TiO$_2$ coexist at the interfaces in the heterostructures, so the following thermodynamic reactions occur during TiO$_2$ growth:

$$TiO_{2-\delta}(s) + VO_2(s) \leftrightarrow TiO_2(s) + VO_{2-\delta}(s) \tag{2}$$
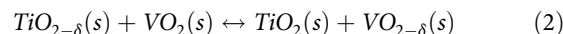
Thermodynamic calculations using this reaction yielded a Gibbs free energy $\Delta G = -18.69$ kJ/mol at $\delta = 0.125$, and −82.77 kJ/mol at $\delta = 0.5$ at $T_G = 150$ °C[40–42]. Regardless of the degree of oxygen deficiency in grown TiO$_{2-\delta}$ layer, oxygen ions tend to transfer spontaneously to the TiO$_2$ layer to equilibrate μ_O between the two layers by forming V_O in VO$_2$ templates. A thermodynamic driving force between TiO$_{2-\delta}$ and VO$_2$ still exists even if few monolayer of TiO$_2$ prevents the direct interface between two dissimilar materials, so "remote" oxygen ionic transport from VO$_2$ to TiO$_{2-\delta}$ is maintained through the few TiO$_2$ monolayer as long as oxygen diffusion is kinetically allowed (Supplementary Figs. 9, 10, 15)[16,43]. To support our observation on the preferred formation of V_O in VO$_2$ templates, we also compared the formation energies of V_O (and vanadium interstitials (V_i)) in rutile VO$_2$ and in TiO$_2$ as a function of Fermi level in the band gap of rutile TiO$_2$ (bottom of Fig. 5c). Our calculations predict that the formation energy of V_O is at
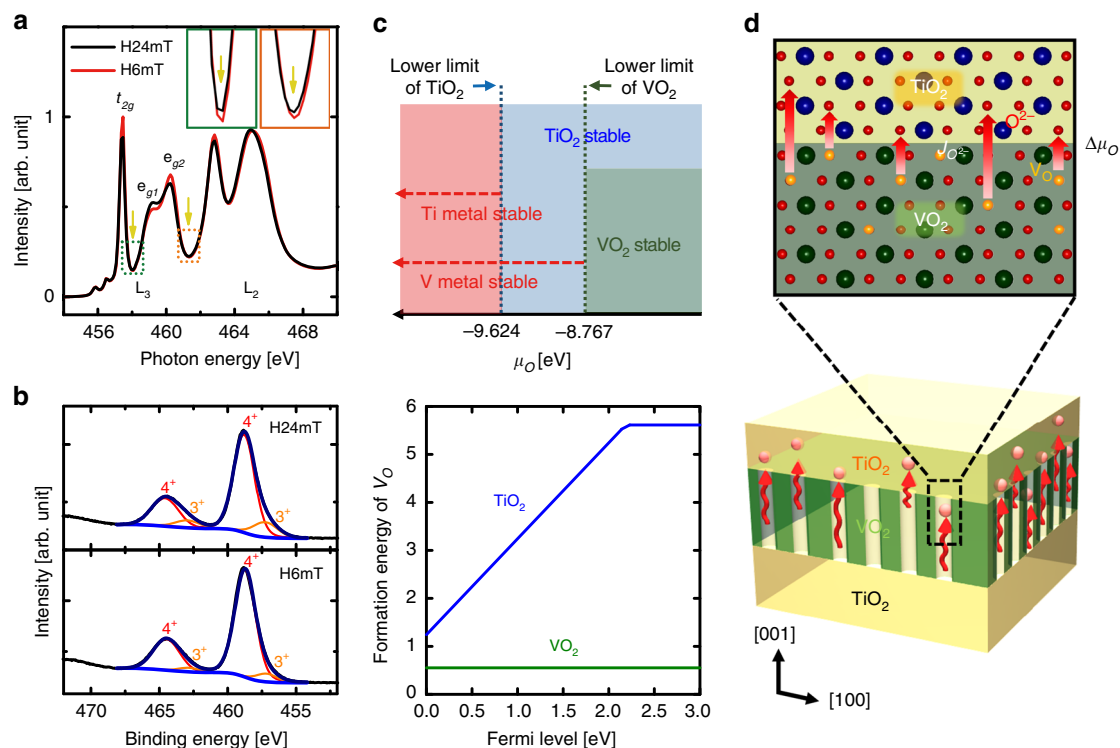
Fig. 5 Facilitated rutile TiO_2 epitaxy by $\Delta\mu_O$ across the TiO_2/VO_2 interface. a Ti L-edge XAS spectra of TiO_2 grown on VO_2 templates under different pO_2 (H24mT, H6mT). The Ti $L_{2,3}$-edge XAS signals from the H6mT were more intense and sharper than from H24mT. **b** XPS spectra of the Ti $2p$ core level of H24mT, H6mT. negligible Ti^{3+} contribution from the H6mT was observed compared to H24mT in TiO_2/VO_2 heterostructures, which reveals the suppression of V_O formation even at the surface of TiO_2 as a result of increased oxygen transport across TiO_2/VO_2 interface under low pO_2. Both XAS and XPS results reveal increased perfection of rutile TiO_2 films after growth at low pO_2. **c** First-principles density functional theory (DFT) calculations to determine values of the lower and upper limit of the chemical potential of μ_O for TiO_2 and VO_2 formation. TiO_2 is the only stable compound at -9.624 eV $\leq \mu_O \leq -8.767$ eV. Comparison of the formation energies of V_O in rutile VO_2 and TiO_2 as a function of Fermi level in the band gap of TiO_2. **d** Increased thermodynamic driving force $\Delta\mu_O$, assisted by high ionic kinetics k, across the interface increased the perfection of registry in the lattice of TiO_2 films by increasing "effective" pO_2 and lowering the activation barrier for epitaxy with concurrent emergence of a metallic $VO_{2-\delta}$ sacrificial templates.

least 0.69 eV lower in VO_2 than in TiO_2 and is ~ 2.0 eV lower that of V_i in VO_2 (Supplementary Fig. 8).

It should be emphasized that the driving force for ionic flux accelerates with increase in the oxygen deficiency on the formed $TiO_{2-\delta}$ layers (i.e., decrease in pO_2 at which the film was grown) by maximizing chemical potential mismatch $(J_{O^{2-}} \propto \Delta G(\text{or } \Delta\mu))$[10]. Due to this strengthened driving force for directional oxygen diffusion from VO_2 to TiO_2, more oxygen vacancies prefer to form in VO_2 templates during TiO_2 growth as pO_2 was decreased. $\Delta\mu_O$ across TiO_2/VO_2 interfaces in the heterostructure drives oxygen flux $(J_{O^{2-}})$ as a directional supply of oxygen ionic radical across the interface from VO_2 sacrificial layers without the dissociation of oxygen gas molecules[10]. The transferred oxygen ions can "effectively" increase the oxygen partial pressure (pO_2) and μ_O at the TiO_2 side; paradoxically, low pO_2 at the ambient is likely to increase "effective" pO_2 ($=$ "external" pO_2 from O_2 gas $+$ "internal" pO_2 across the solid-solid interface) during TiO_2 growth on VO_2 templates. As a result, the increased "effective" pO_2 by the enhanced $J_{O^{2-}}$ across the interface magnifies driving force for the formation of rutile TiO_2 with stoichiometry in heterostructure (Supplementary Fig. 16); lack of oxidation in the deposited $TiO_{2-\delta}$ species during the growth is compensated by transferred oxygen ions from the VO_2 templates below[10,44].

For heterogenous nucleation on the substrate during the film growth, the activation energy (ΔG^*) for the formation of crystalline nuclei could be significantly lowered by increasing the supply of oxygen ions (i.e., increasing the driving force for

formation of rutile TiO_2) based on the following expression[45].

$$\Delta G^* = \frac{16\pi\gamma_{fv}^3}{3(\Delta G_v - \Delta G_S)^2} S(\theta) \quad (3)$$

where ΔG_v, γ_{fv}, ΔG_S, and $S(\theta)$ are the chemical free energy change for the formation of solid rutile TiO_2 nuclei, surface free energies, interfacial strain energy and a geometrical factor for heterogeneous nucleation, respectively. At very low $T_G \sim 150\,°C$, the adatoms freeze in metastable form, so the time constant for crystallization $(\tau_{cryst}, \text{i.e., } \frac{1}{\tau_{cryst}} = A \cdot \exp\left(-\frac{\Delta G^*}{k_B T_g}\right))$ becomes extremely long due to the high ΔG^* and insufficient thermal energy; the amorphized or metastable TiO_2 films (with nonequilibrium structure) are likely to form due to the kinetic hindrance of crystal formation (e.g., insufficient movement of ablated TiO_2 adatoms and/or limited reaction with O_2 gas) as observed in our TiO_2/TiO_2 homostructure.

In our case, VO_2 sacrificial layers from the bottom acts as epitaxial templates for rutile TiO_2. They also sacrifice themselves by forming V_O in VO_2 and thereby supply high concentration of oxygen ions to $TiO_{2-\delta}$ by magnifying the driving force for the oxygen transport at the VO_2/TiO_2 interfaces. Since γ_{fv} and ΔG_S are unlikely to be changed regardless of the existence of VO_2 templates (Supplementary Fig. 6 and Fig. 15), greater ΔG_v induced by $J_{O^{2-}}$ significantly reduce ΔG^* in heterostructure than in homostructure. As a result, the large reduction of τ_{cryst} by the decrease in ΔG^* enables unprecedented epitaxy of high-temperature-stabilized TiO_2 rutile phase[19,23] at extremely low

$T_G \sim 150\,°C$ by changing the initial stoichiometry of two oxides with different μ across the interface.

In addition to thermodynamic viewpoint, the transport of charged oxygen ions is kinetically facilitated along the crystallographic [001] direction, which has open channels in anisotropic rutile VO_2 and TiO_2[15,16]. One-dimensional empty channels are aligned along the c axis in our TiO_2/VO_2 heterostructures and provide the advantage of removing significant amounts of oxygen ions due to a high oxygen diffusion coefficient. Thus, the growth direction of [001] TiO_2 films should strongly accelerate the out-diffusion kinetics of oxygen transport (increased k in Fig. 1a) from the VO_2 sacrificial templates as a result of mismatch in chemical potential ($\Delta\mu_O$ in Fig. 1a); significant reduction in oxygen transport across the oxide interface along the [001] direction kinetically facilitates the decrease in ΔG^* for nucleation of rutile TiO_2 phase even at low T_G to support epitaxial growth of rutile TiO_2 films on VO_2 templates.

On the other hand, the kinetics of oxygen transport will eventually limit our epitaxial growth based on "internal" oxygen transport across the TiO_2/VO_2 interface (Supplementary Figs. 11, 12, 13). Since the oxygens should be supplied from the TiO_2/VO_2 interfaces through the intervening TiO_2 layers, the thickness of "epitaxial" TiO_2 will be limited by oxygen diffusion through the intervening TiO_2 layer. In fact, while the "epitaxial" thickness linearly increased with growth time in the TiO_2 films grown at 300 °C, the "epitaxial" thickness appears to be saturated to be ~ 10 nm as a "critical" thickness at $t_{film} > 10$ nm at $T_G \sim 150\,°C$ due to scarce source of "internal" oxygen transport ($J_{O^{2-}}$) even if the growth time increases (Supplementary Fig. 11). Therefore, the existence of "critical" thickness provides the convincing evidence of our unprecedented low-temperature epitaxy driven by direction oxygen ionic transport.

In summary, unconventional low-temperature epitaxy of rutile TiO_2 films was achieved by exploiting the directional transport of oxygen ions across TiO_2/VO_2 heterointerfaces. The thermodynamic driving force, assisted by facile ionic pathway along oxygen channel, across the interface enabled more perfect registry in the lattice of TiO_2 films by lowering the activation barrier for stable nuclei, with concurrent emergence of a metallic TiO_2/VO_2 heterostructures. Contrary to typical experimental condition to obtain TiO_2 with better stoichiometry, interestingly, V_O formation was diminished under low external pO_2, because the accelerated chemical potential mismatch ($\Delta\mu_O$) under low external pO_2 significantly increased "effective" pO_2 by the internal oxygen transport across the TiO_2/VO_2 interface. Therefore, the controlled ionic transport by $\Delta\mu_O$ may offer an opportunity to design a new heterostructure with different degree of freedom at the interfaces as a result of tuning of ionic defects, and also to stabilize thermal-energy-requiring phases simply by interfacing with dissimilar materials with different thermodynamic and kinetic driving force of ionic defects.

Methods

Synthesis of epitaxial TiO_2/VO_2 heterostructures on TiO_2 substrates. Epitaxial VO_2 thin films (10–14 nm thick) were grown on (001) TiO_2 single-crystal substrates, followed by the growth TiO_2 films (2.5–60 nm thick) by pulsed laser deposition (PLD). The stoichiometric targets for the synthesis of heterostructures were prepared by sintering stoichiometric powders of V_2O_5 (99.99%, Sigma Aldrich) at 600 °C for 6 h and TiO_2 (99.95%, Sigma Aldrich) at 1100 °C for 4 h. First, (001) TiO_2 single crystal substrates (Shinkosha CO., LTD) were loaded into the PLD chamber, which was then evacuated to a base pressure of $\sim 1 \times 10^{-6}$ Torr. Then, the rotating V_2O_5 targets were ablated by focusing KrF excimer laser (Coherent Compex Pro 102 F, $\lambda = 248$ nm) with a fluence of 1 J/cm² and repetition rate of 1 Hz. The VO_2 growth was performed at fixed $pO_2 = 12$ mTorr and 300 °C, which was selected to induce a steep metal-insulator transition near room temperature from coherently tensile-strained VO_2 films. After VO_2 growth, the substrate temperature was quenched to 50 ~ 150 °C. Subsequently, TiO_2 films were grown on VO_2 templates under 6 mTorr $\le pO_2 \le$ 24 mTorr to control the

thermodynamic driving force for oxygen ionic transport across the interface at low temperature ($T_G = 50–150$ °C). After the growth of heterostructures, the samples were cooled down to room temperature with rate of 20 °C/min.

Structural and electrical characterization of heterostructures. To characterize crystal-structure modulation in $TiO_2/VO_2/TiO_2$ heterostructures with different degrees of chemical potential mismatch using pO_2 during TiO_2 growth, high-resolution X-ray scattering measurements were performed using synchrotron radiation at 3A MP-XRS ($\lambda \sim 0.11145$ nm, energy ~ 11,125 keV at Si (111)) and at 3D XRD ($\lambda \sim 0.12398$ nm, energy ~ 10 keV at Si (111) beamline of Pohang Light Source-II (PLS-II, Pohang, Republic of Korea), and using an in-house HRXRD (Bruker Discover 8 X-ray diffractometer) with Cu $K_{\alpha 1}$ radiation ($\lambda = 0.15406$ nm). The detailed information on in-plane and out-of-plane lattice parameters and strain states of each film in the heterostructures were obtained by using both symmetric 2θ-ω scan and asymmetric reciprocal space mapping (RSM) around the (112) reflection. The simulation of symmetric 2θ-ω scans was performed using LEPTOS software program. The surface morphology of the films was observed using an atomic force microscope (AFM, VEECO Dimension 3100).

For atomic resolution analysis of crystal structure, the samples were prepared using a dual-beam focused ion beam (FIB) system (Helios G3, FEI). HRTEM and STEM analyses (JEM-ARM200F, JEOL) were performed at 200 kV equipped with a 5th order aberration corrector (ASCOR, CEOS GmbH) for forming 0.7 Å probe. The collection semi-angles were 68 to 280 mrad for HAADF, 27 to 110 mrad for LAADF and 10 to 20 mrad for ABF. The obtained raw images were band-pass filtered to reduce background noise (HREM Research Inc.).

The sheet resistance R_S was measured as a function of temperature during the heating and cooling from 250K to 340K using Hall measurement system. Measurements were carried out in van der Pauw geometry with square samples (5 mm × 5 mm) and indium Ohmic contacts (<1 mm × 1 mm) in the sample corners. The four-terminal resistances were measured using a 10-µA current.

To investigate electronic structure of TiO_2/VO_2 heterostructures, X-ray absorption spectroscopy (XAS) and linear dichroism (XLD) were performed using high sensitivity at the 2A MS beamline at PLS-II. The total electron yield mode with an energy resolution of ~0.1 eV was used for both measurements at a base pressure of 5×10^{-10} Torr in the analysis chamber by measuring the sample current (I_I) divided by the beam current (I_o) to remove the variation of beam intensity. The linear dichroism of V $L_{2,3}$-edge was carried out by using horizontally-polarized or vertically-polarized X-ray beams with photon incidence angle of 22.5° at the measurement temperatures below (270 K) and above the T_{MI} (320 K) of as-grown VO_2 films. And then, the Ti $L_{2,3}$-edges XAS measurements were performed on $TiO_2/VO_2/TiO_2$ heterostructures; photon incidence angle was 45°, and measurement temperatures were 270 K and 320 K. Due to its element-resolved characterization with several nanometer probing depth, Ti $L_{2,3}$-edges spectra were obtained only from the TiO_2 epitaxial films on top.

To evaluate the surface stoichiometry of the TiO_2 rutile films as a result of directional oxygen transport from VO_2 films in our $TiO_2/VO_2/TiO_2$, XPS spectra of Ti $2p$ core level were acquired on the 4A2 SARPES and 4D PES beam line (PLS-II) in an ultra-high vacuum chamber (2×10^{-10} Torr). Before measurement, we carefully removed possible contaminants by using gentle Ar surface treatment. Ion sputtering was performed for 4 min and 20 min in the preparation chamber under the Ar pressure of 8×10^{-6} Torr at anode voltage of 500V and 2.5 kV. For collect Ti 3d spectra, we measured from 475 eV to 445 eV with 50-meV steps at 300 K. The measured spectra were deconvoluted using XPSPEAK41 software.

First-principles calculation. First-principles density functional theory (DFT) calculations were performed using the Projector Augmented Wave (PAW) method and the generalized gradient approximation of Perdew, Burke, and Ernzerhof (PBE) for the exchange-correlation potential as implemented in Vienna Ab-initio Simulation Package (VASP) code[46]. Periodic boundary condition and Monkhorst-Pack k-point sampling with a Γ-centered k-point grid of up to $8 \times 8 \times 8$ was used for the Brillouin zone integration. An energy cutoff of 450 eV was used for the plane-wave representation of the wavefunctions and the 3s electrons of V and Ti ions were considered as valence electrons. A Hubbard U correction term was applied to the V ($U = 3.25$ eV) and Ti ($U = 3.00$ eV) to properly reproduce the strong on-site Columbic repulsion of 3d-electrons[47]. Atomic structures were relaxed until all Hellman-Feynman forces were below 0.01 eV/Å. The optimized lattice parameters are $a = 4.67$ Å and $c = 2.52$ Å for Ti metal and $a = 3.31$ Å for V metal. The optimized lattice parameters are $a = 4.559$ Å and $c = 2.889$ Å for rutile VO_2, and $a = 4.608$ Å and $c = 2.989$ Å for rutile TiO_2.

Data availability
The authors declare that the all the data supporting the finding of this study are available within this article and its Supplementary Information files, and are available from the corresponding author on reasonable request.

References

1. Kroemer, H. Nobel lecture: quasielectric fields and band offsets: teaching electrons new tricks. *Rev. Mod. Phys.* **73**, 783–793 (2001).
2. Dingle, R., Stormer, H. L., Gossard, A. C. & Wiegmann, W. Electron mobilities in modulation-doped semiconductor heterojunction superlattices. *Appl. Phys. Lett.* **33**, 665 (1978).
3. Ohtomo, A. & Hwang, H. Y. A high-mobility electron gas at the $LaAlO_3$/$SrTiO_3$ heterointerface. *Nature* **427**, 423 (2004).
4. Lee, D. et al. Isostructural metal-insulator transition in VO_2. *Science* **362**, 1037–1040 (2018).
5. Li, Y. Y. & Chueh, W. C. Electrochemical and chemical insertion for energy transformation and switching. *Annu. Rev. Mater. Res.* **48**, 137–165 (2018).
6. Tsui, D. C., Stormer, H. L. & Gossard, A. C. Two-dimensional magnetotransport in the extreme quantum limit. *Phys. Rev. Lett.* **48**, 1559 (1982).
7. Morkoc, H. & Solomon, P. M. The HEMT: a superfast transistor. *IEEE Spectr.* **21**, 28–35 (1984).
8. Fuller, E. J. et al. Li-ion synaptic transistor for low power analog computing. *Adv. Mater.* **29**, 1604310 (2017).
9. Jeong, J. et al. Suppression of metal-insulator transition in VO_2 by electric field–induced oxygen vacancy formation. *Science* **339**, 1402–1405 (2013).
10. Guo, E. J. et al. Oxygen diode formed in nickelate heterostructures by chemical potential mismatch. *Adv. Mater.* **30**, 1705904 (2018).
11. Veal, B. W. et al. Interfacial control of oxygen vacancy doping and electrical conduction in thin film oxide heterostructures. *Nat. Commun.* **7**, 11892 (2016).
12. Scheiderer, P. et al. Tailoring materials for mottronics: excess oxygen doping of a prototypical mott insulator. *Adv. Mater.* **30**, 1706708 (2018).
13. Lee, S. W., Liu, Y. Q., Heo, J. & Gordon, R. G. Creation and control of two-dimensional electron gas using Al-based amorphous oxides/$SrTiO_3$ heterostructures grown by atomic layer deposition. *Nano Lett.* **12**, 4775–4783 (2012).
14. Leighton, C. Electrolyte-based ionic control of functional oxides. *Nat. Mater.* **18**, 13–18 (2019).
15. Jeong, J. et al. Giant reversible, facet-dependent, structural changes in a correlated-electron insulator induced by ionic liquid gating. *Proc. Natl. Acad. Sci. USA* **112**, 1013–1018 (2015).
16. Passarello, D., Altendorf, S. G., Jeong, J., Samant, M. G. & Parkin, S. S. P. Metallization of epitaxial VO_2 films by ionic liquid gating through initially insulating TiO_2 layers. *Nano Lett.* **16**, 5475–5481 (2016).
17. Yoon, H. et al. Reversible phase modulation and hydrogen storage in multivalent VO_2 epitaxial thin films. *Nat. Mater.* **15**, 1113–1119 (2016).
18. Yoon, H., Park, J., Choi, S.-Y., Lee, D. & Son, J. Facet-dependent phase control by band filling and anisotropic electron-lattice coupling in HVO_2 epitaxial films. *Adv. Electron. Mater.* **4**, 1800128 (2018).
19. Mitsuhashi, T. & Kleppa, O. J. Transformation enthalpies of the TiO_2 polymorphs. *J. Am. Ceram. Soc.* **62**, 356–357 (1978).
20. Ranade, M. R. et al. Energetics of nanocrystalline TiO_2. *Proc. Natl. Acad. Sci. USA* **99**, 6476–6481 (2002).
21. Bayati, M. R., Joshi, S., Narayan, R. J. & Narayan, J. Low-temperature processing and control of structure and properties of TiO_2/c-sapphire epitaxial heterostructures. *J. Mater. Res.* **28**, 1669–1679 (2013).
22. Chen, S. et al. Ultrahigh-vacuum metalorganic chemical-vapor-deposition growth and in-situ characterization of epitaxial TiO_2 films. *J. Vac. Sci. Technol. A* **11**, 2419–2429 (1993).
23. Hanaor, D. A. H. & Sorrell, C. C. Review of the anatase to rutile phase transformation. *J. Mater. Sci.* **46**, 855–874 (2010).
24. Muller, D. A., Nakagawa, N., Ohtomo, A., Grazul, J. L. & Hwang, H. Y. Atomic-scale imaging of nanoengineered oxygen vacancy profiles in $SrTiO_3$. *Nature* **430**, 657–661 (2004).
25. Zhou, H., Chisholm, M. F., Gupta, A., Pennycook, S. J. & Narayan, J. Two-dimensional metamaterials for epitaxial heterostructures. *Curr. Opin. Solid State Mater. Sci.* **18**, 46–52 (2014).
26. Fan, L. L. et al. Strain dynamics of ultrathin VO_2 film grown on TiO_2 (001) and the associated phase transition modulation. *Nano Lett.* **14**, 4036–4043 (2014).
27. Yang, M. et al. Suppression of structural phase transition in VO_2 by epitaxial strain in vicinity of metal-insulator transition. *Sci. Rep.* **6**, 23119 (2016).
28. Zhang, J. et al. Evolution of structural and electrical properties of oxygen-deficient VO_2 under low temperature heating process. *ACS Appl. Mater. Interfaces* **9**, 27135–27141 (2017).
29. Abbate, M. et al. Soft-x-ray-absorption studies of the electronic-structure changes through the VO_2 phase transition. *Phys. Rev. B* **43**, 7263–7266 (1991).
30. Aetukuri, N. B. et al. Control of the metal–insulator transition in vanadium dioxide by modifying orbital occupancy. *Nat. Phys.* **9**, 661–666 (2013).
31. Haverkort, M. W. et al. Orbital-assisted metal-insulator transition in VO_2. *Phys. Rev. Lett.* **95**, 196404 (2005).
32. Zhang, Z. et al. Evolution of metallicity in vanadium dioxide by creation of oxygen vacancies. *Phys. Rev. Appl.* **7**, 034008 (2017).
33. Karel, J. et al. Distinct electronic structure of the electrolyte gate-induced conducting phase in vanadium dioxide revealed by high-energy photoelectron spectroscopy. *ACS Nano* **8**, 5784–5789 (2014).
34. Krüger, P. Multichannel multiple scattering calculation of $L_{2,3}$-edge spectra of TiO_2 and $SrTiO_3$: Importance of multiplet coupling and band structure. *Phys. Rev. B* **81**, 125121 (2010).
35. Kucheyev, S. O. et al. Electronic structure of titania aerogels from soft x-ray absorption spectroscopy. *Phys. Rev. B* **69**, 245102 (2004).
36. Chen, C. L. et al. Electronic properties of free-standing TiO_2 nanotube arrays fabricated by electrochemical anodization. *Phys. Chem. Chem. Phys.* **17**, 22064–22071 (2015).
37. Chen, C., Avila, J., Frantzeskakis, E., Levy, A. & Asensio, M. C. Observation of a two-dimensional liquid of Frohlich polarons at the bare $SrTiO_3$ surface. *Nat. Commun.* **6**, 8585 (2015).
38. Biesinger, M. C., Lau, L. W. M., Gerson, A. R. & Smart, R. S. C. Resolving surface chemical states in XPS analysis of first row transition metals, oxides and hydroxides: Sc, Ti, V, Cu and Zn. *Appl. Surf. Sci.* **257**, 887–898 (2010).
39. Ohtomo, A. & Hwang, H. Y. Growth mode control of the free carrier density in $SrTiO_{3-\delta}$ films. *J. Appl. Phys.* **102**, 083704 (2007).
40. Waldner, P. & Eriksson, G. Thermodynamic modelling of the system titanium-oxygen. *Calphad* **23**, 189–218 (1999).
41. Okinaka, H., Kosuge, K. & Kachi, S. Phase equilibria and thermodynamic properties in the V_nO_{2n-1} system. *J. Jpn. Inst. Met.* **12**, 44–48 (1971).
42. Knacke O., Kubaschewski O. & Hesselmann K. *Thermochemical Properties of Inorganic Substances* (Springer, 1991).
43. Kim, H., McIntyre, P. C., Chui, C. O., Saraswat, K. C. & Stemmer, S. Engineering chemically abrupt high-k metal oxide/silicon interfaces using an oxygen-gettering metal overlayer. *J. Appl. Phys.* **96**, 3467–3472 (2004).
44. Zhu, J. X. et al. Probing vacancy behavior across complex oxide heterointerfaces. *Sci. Adv.* **5**, eaau8467 (2019).
45. Ohring M. *Materials Science of Thin Films*. (Academic Press, 1991).
46. Perdew, J. P., Burke, K. & Ernzerhof, M. Generalized gradient approximation made simple. *Phys. Rev. Lett.* **77**, 3865–3868 (1996).
47. Hautier, G., Ong, S. P., Jain, A., Moore, C. J. & Ceder, G. Accuracy of density functional theory in predicting formation energies of ternary oxides from binary oxides and its implication on phase stability. *Phys. Rev. B* **85**, 155208 (2012).

Author contributions

J.S., Y.P., M.J. and D.Y. conceived the idea and designed the study; Y.P. and M.J. performed the film growth, X-ray diffraction, transport measurement with the assistance of D.Y. and H.H.; Y.P. and M.J. performed the synchrotron x-ray spectroscopy with the assistance of Y.K.; H.S., G.-Y.K., K.S. and S.-Y.C. characterized the samples by scanning transmission electron microscopy; D.L. performed first-principles calculations; J.S. and Y.P. wrote the manuscript and all authors commented on it; J.S. directed the overall research.

Competing interests

The authors declare no competing interests.

Additional information

Supplementary information is available for this paper at https://doi.org/10.1038/s41467-020-15142-x.

Correspondence and requests for materials should be addressed to J.S.

Peer review information *Nature Communications* thanks the anonymous reviewers for their contribution to the peer review of this work.

Reprints and permission information is available at http://www.nature.com/reprints

Publisher's note Springer Nature remains neutral with regard to jurisdictional claims in published maps and institutional affiliations.